Intensity invariant complex encoded colour correlation

Article (Accepted Version)

Intensity Invariant Complex Encoded Colour Correlation

Philip Birch*

Dept. of Engineering and Design, University of Sussex, Falmer, East Sussex, BN1 9QT, UK

**Corresponding author: p.m.birch@sussex.ac.uk*

Optical correlation has traditionally processed monochromatic grey scale images. This paper develops a new encoding mechanism that uses the chromaticy of the input signal. It is then not only possible to detect different coloured objects but the system is invariant to changes in the brightness of the lighting, including variations across the object.

OCIS codes: 070.4550 , 330.1690.

1. Introduction

Correlation for pattern recognition is a process of comparing two signals and it is commonly used in target detection. Historically the method was implemented as a $4-f$ correlator or joint transform correlator (JTC) architecture, increasingly this has been replaced by digital methods employing the fast Fourier transform (FFT). Typically correlation has been used on monochromatic grey-level signals. The extra colour information in the image is usually discarded to produce a monochromatic correlator due to the difficultly encoding a three dimensional signal onto both a two dimensional input spatial light modulator (SLM) and a two dimensional filter SLM. In addition, since the correlation is realised by Fourier transforms, it is not possible to normalise the intensity locally as can be done in the space domain correlation. This leads to the false classification of bright objects within the image. Correlation performed with a degree of invariance to intensity (both global and local) is therefore desirable. It can be partially achieved by high pass filtering of the signal, but this does not take into account any intensity variations across the object.

There has however been interest in the past in correlating polychromatic signals. This has been achieved by encoding the data onto red, green and blue channels or some some other colour space [1]. The data is parallelised but it is still effectively treating each colour as a separate correlation and combining the correlation plane results. Colour JTC have been shown by Yu *et al* [2] and Hsieh *et al* [3], quaternion and hyper-complex Clifford algebras

Accepted for publication in Applied Optics 2012

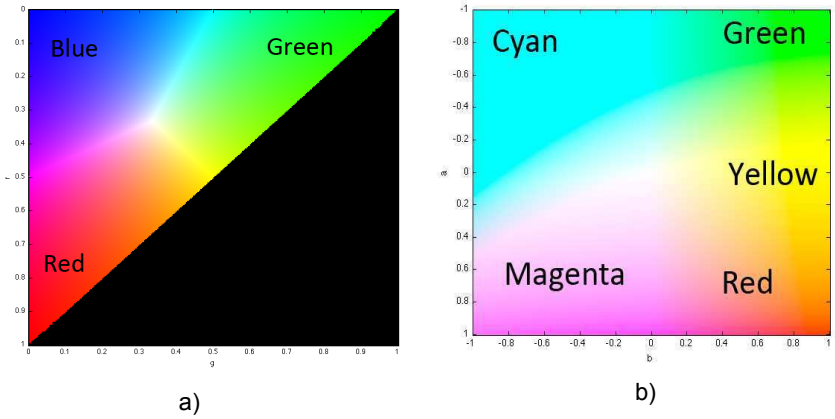

Fig. 1. a) Chroma values displayed as colours. Note, since $r + g + b = 1$ some values are not possible (indicated in black), b) Lab colour space with L=100.

have been successfully demonstrated for colour manipulation [4], image registration [5] and correlation [6] [7] [8] but since the data remains three dimensional, they are physically more difficult to realise in an optical system and when implemented on a computer they often involve multiple FFTs of the data, making them slow.

This paper demonstrates a simple way of encoding colour information that can be implemented on a spatial light modulator or via a high speed FFT operation on an electronic processor. Unlike hyper complex or Clifford algebra approaches only the chromaticity channels are utilised and the intensity channels are dropped. We have found this gives a better performance when the lighting varies across the object.

There are several colour spaces available for use. Typically a CCD camera captures colour information by the use of a Bayer filter. This is converted into the three dimensional RGB space which consists of three concatenated two dimensional images containing the red, green and blue channels. Other colour spaces such as HSV, Lab and YCrCb separate out the intensity information from the colour channels. This separation has a desirable effect in many object matching applications in that the lighting variation is at least partially contained on one channel. Thus by neglecting the intensity values we can gain two advantages: the changes in the system due to lighting variations are partially removed; and the colour information can now be contained in only two dimensions. Complex encoding (phase and amplitude) enables all dimensionality to be physically realisable with SLMs.

This paper will demonstrate a proof of principle of this operation for two colour spaces.

2. Chroma Space Complex Encoding

In RGB colour space the colour channels are represented by **R**, **G**, **B**. The RG chroma values are calculated as

$$\mathbf{r} = \frac{\mathbf{R}}{\mathbf{R}+\mathbf{B}+\mathbf{G}} \tag{1}$$

and

$$\mathbf{g} = \frac{\mathbf{G}}{\mathbf{R}+\mathbf{B}+\mathbf{G}} \tag{2}$$

Note that a blue chroma value is redundant since it can be calculated from $\mathbf{b} = 1 - \mathbf{r} - \mathbf{g}$. The reduction to two dimension means the colour data can now be encoded as a complex data. The chroma mapping is shown in figure 1 a).

$$\mathbf{c} = \mathbf{r} + i\mathbf{g} \tag{3}$$

If $R = G = B = 0$, $\mathbf{r}$ and $\mathbf{g}$ are undefined. In this case $\mathbf{c}$ is set to zero. A frequency domain correlation can then calculated as

$$\xi = |\mathcal{F}^{-1}\{\mathbf{I}_c(u,v)\mathbf{F}_c^*(u,v)\mathbf{G}(u,v)\}|^2 \tag{4}$$

where $\mathcal{F}$ is the Fourier transform operator, $\mathbf{F}$ is the filter and $\mathbf{I}$ is the Fourier transform of the input signal. The c subscript indicates the complex encoding shown in equation 3. The matched filter alone is very poor at target discrimination. To improve this the image was filtered by $\mathbf{G}(u,v)$, the Fourier domain difference of Gaussian (DOG) wavelet filter as described in [9] [10].

$$\mathbf{G}(k) = \frac{1}{2\pi}\left(\exp\left(-k^2\sigma_1^2/2\right) - \exp\left(-k^2\sigma_2^2/2\right)\right) \tag{5}$$

where k is radial frequency.

If we consider two signals we wish to correlate, $c_1(\mathbf{x})$ and $c_2(\mathbf{x})$, the result will be given by

$$\xi(\mathbf{x}) = c_1(\mathbf{x}) \odot c_2(\mathbf{x}) \tag{6}$$

$$= |c_1(\mathbf{x})| \exp(i\theta_1(\mathbf{x})) \odot |c_2(\mathbf{x})| \exp(i\theta_2(\mathbf{x})) \tag{7}$$

where θ_1 and θ_2 are the phase angles of $c_1(\mathbf{x})$ and $c_2(\mathbf{x})$ respectively, $\mathbf{x}$ is a two dimensional co-ordinate and $\odot$ is the two dimensional correlation operator. If we assume that the objects are uniform in colour then

$$\xi(\mathbf{x}) = |c_1(\mathbf{x})| \exp(i\theta_1) \odot |c_2(\mathbf{x})| \exp(i\theta_2) \tag{8}$$

$$= |c_1(\mathbf{x})| \odot |c_2(\mathbf{x})| \times \exp\left(i\left(\theta_1 - \theta_2\right)\right) \tag{9}$$

It can be see that the phase information is required to differentiate colours. We therefore conclude that instead of the traditional intensity peak threshold to determine if a match has

occurred we have to add the additional constraint that peaks imaginary component must be less than some threshold, $\alpha_{\mathbb{I}}$.

We note though that this is worst case, for multi-coloured objects the approximation that produces equation 9 does not hold and we must consider the cross-correlation of the amplitude and phase signals. In this case the phase of the output correlation plane is no longer required.

3. L*a*b* Colour Space

Since the chroma space encoding is not valid for $r + b > 1$, this is wasteful of a large part of the potential spatial bandwidth of an SLM. To utilise more of the spatial bandwidth the L*a*b* colour space has also been investigated. This colour space separates brightness, L and two colour channels, a and b. To implement this in $2D$ the L is set to its maximum value, 100. The gamut for $L = 100$ is shown in figure 1 b). The image was converted to this space by encoding it as:

$$\mathbf{c_{Lab}} = \mathbf{a} + i\mathbf{b} \tag{10}$$

and the correlation experiments were repeated using the same process described by equation 4 expect that the c subscript indicates the complex encoding is now provided by equation 10. The results are shown in the next section.

4. Results

The input image is shown in figure 2. The target was the two green tanks orientated horizontally. Figure 3 a) is the DOG filtered correlation output (real only) for chroma encoding. The two sharp peaks correspond to the two identical target tanks and the red tank is rejected because of its colour and the tilted tank is rejected to the lack of rotational invariance in such a filter. Figure 3 b) shows the equivalent results for the Lab encoded correlation.

Figure 4 shows an example of multiple targets. The image is generated by taking the original tank image and altering the hue, saturation and brightness value of each tank and pasting this onto a cluttered background image. Ideally, the filter should only return a peak in the results for the top row of tanks since these tanks have identical hues but differ in brightness to the original target. Figure 5 shows the absolute value of the correlation output plane. The correlator clearly fails to distinguish between the green and blue colours. Figure 6 and figure 7 shows the real and an imaginary components of the correlation output. It is clearly possible to distinguish the colours by taking peaks with zero phase, i.e., all the power is contained in the real only component of the output. This occurs on the top row of peaks in figure 6 which correspond to the tanks with same hue and saturation as the target tank.

To test the tolerance of the scheme's false colour rejection ability, a single tank was pasted into the same background as used in figure 2. The tank's hue, saturation, and values were

Fig. 2. Input image. The targets are the green horizontal tanks.

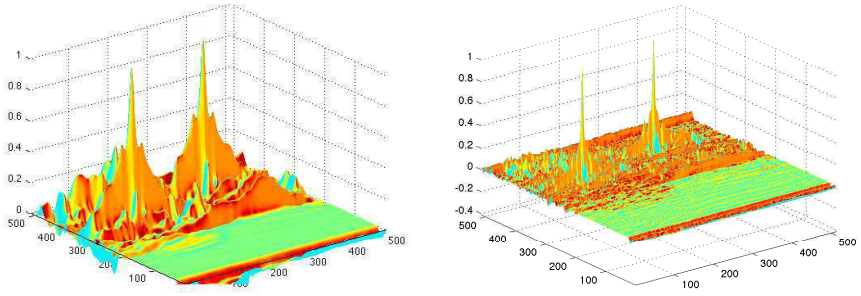

Fig. 3. a) Chroma encoded DOG filter result. b) LAB encoded DOG filter result.

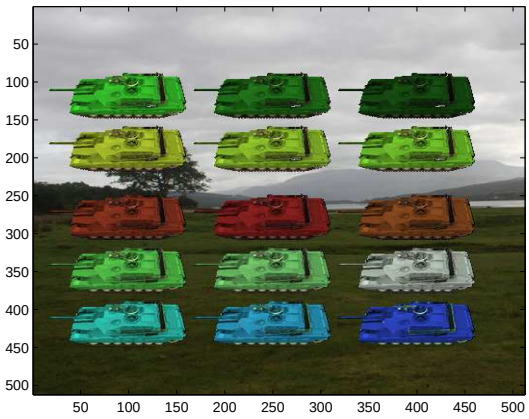

Fig. 4. Input image with multiple targets. The top row of tanks have the same hue and saturation but varying in value. In the second and fourth row, hue and value are constant but the saturation is decreased. In the third row hue and value is changed and in the fifth row hue alone is changed.

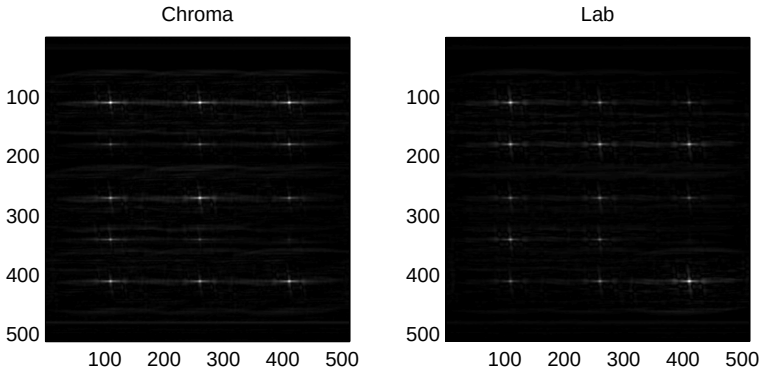

Fig. 5. Absolute component of the correlation output for the chroma and Lab colour encoding

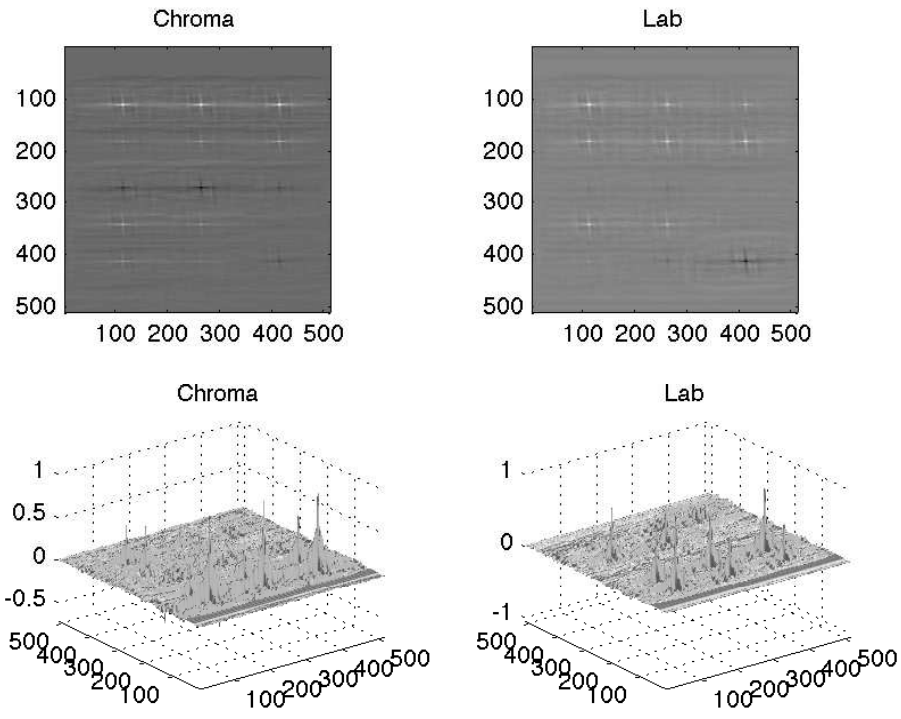

Fig. 6. Real component of the correlation output for the chroma and Lab colour encoding.

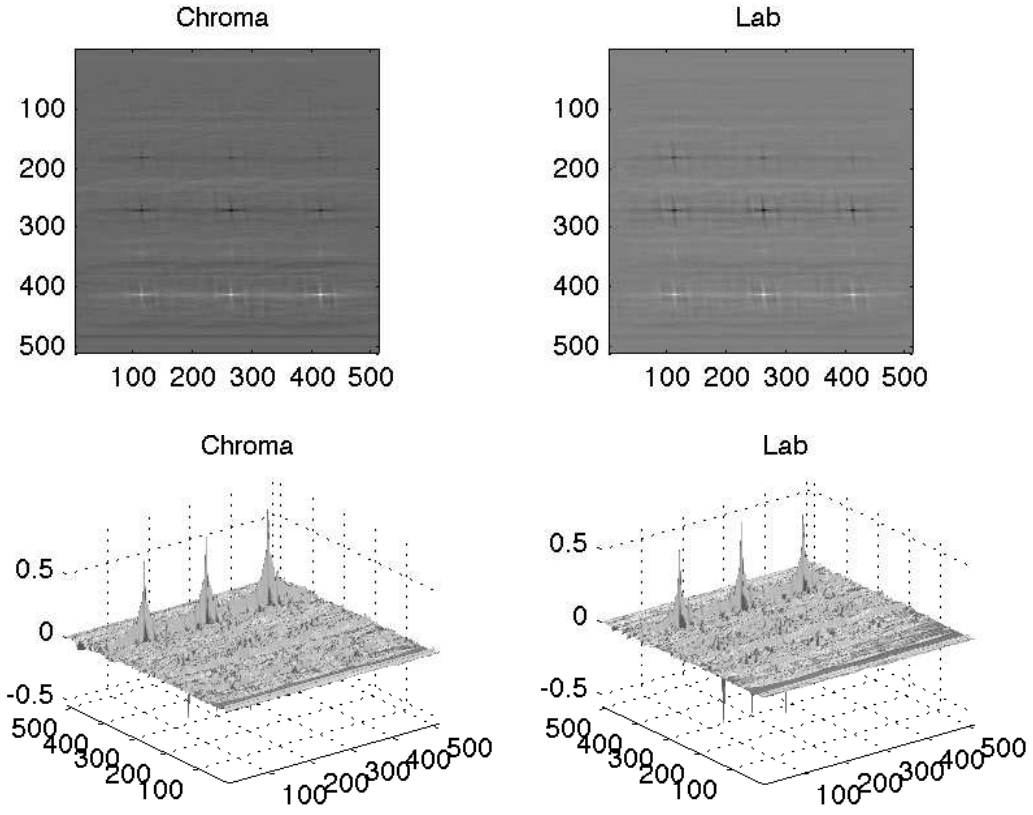

Fig. 7. Imaginary component of the correlation output for the chroma and Lab colour encoding.

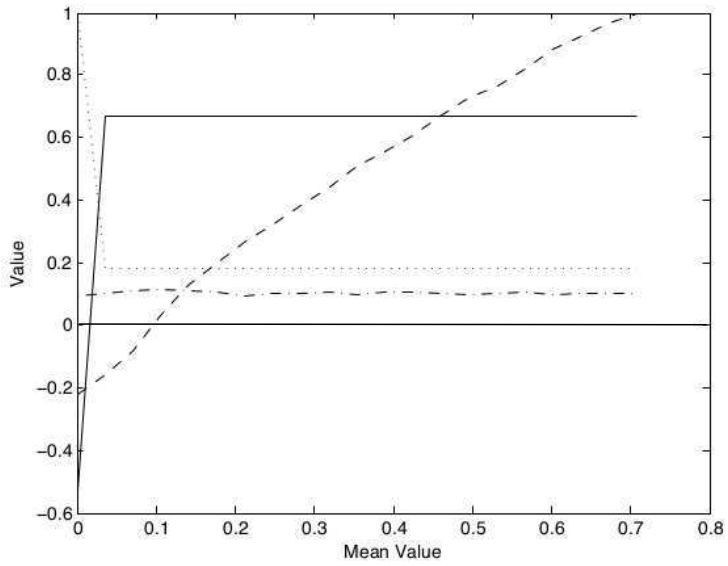

Fig. 8. Plot of the mean value versus COPA. The chroma encoded real COPA: solid line; chroma encoded imaginary COPA: dotted line; Lab encoded real COPA: dashed line; Lab encoded imaginary COPA: dot-dash line

then altered by applying a multiplier to each channel and the mean value of this across the whole tank was calculated. The mean was used since there is a degree of variation across the whole tank image in all of the parameters. The values were then plotted against the COPA (correlation output peak amplitude), which has been split into its real and imaginary components. Thus, to get the COPI (correlation output peak intensity), the real and imaginary results need to be squared and added together. For reference, with the multiplier set to 1 the mean value was 0.35, the mean hue was 0.29 and the mean saturation was 0.72

Figure 8 shows the COPA as the tank's brightness value is altered. It can be seen that the chroma encoded correlation is largely invariant to intensity changes. This is an important result since it means the correlator is now illumination brightness invariant. The results for the Lab encoded filter do not exhibit this ability.

Figure 9 shows the results of the saturation channel been altered. It can be seen that both the chroma and Lab encoded filters are less robust to saturation changes.

Figure 10 shows the results for the hue channel alteration. Here we do not desire invariance since we wish to distinguish colours.

Multiple coloured versions of the tank have been tested. Figure 11 shows a green tank and multicolour tank. The multicoloured tank is the target and the intensity output from

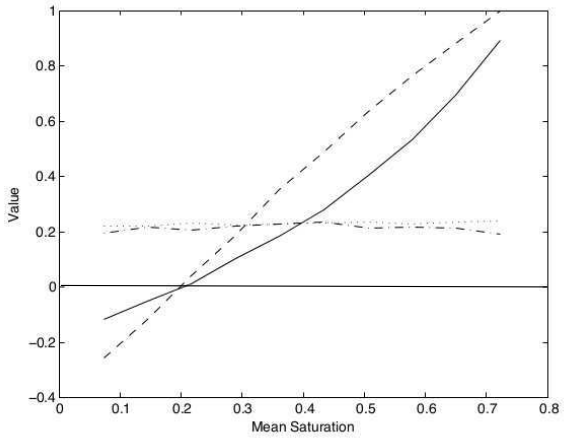

Fig. 9. Plot of the mean saturation versus COPA. The chroma encoded real COPA: solid line; chroma encoded imaginary COPA: dotted line; Lab encoded real COPA: dashed line; Lab encoded imaginary COPA: dot-dash line

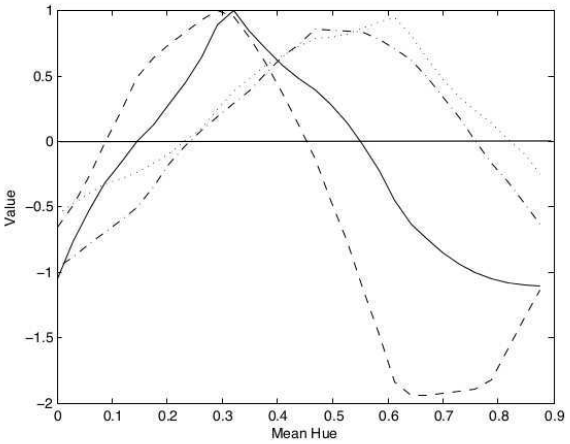

Fig. 10. Plot of the mean hue versus COPA. The chroma encoded real COPA: solid line; chroma encoded imaginary COPA: dotted line; Lab encoded real COPA: dashed line; Lab encoded imaginary COPA: dot-dash line

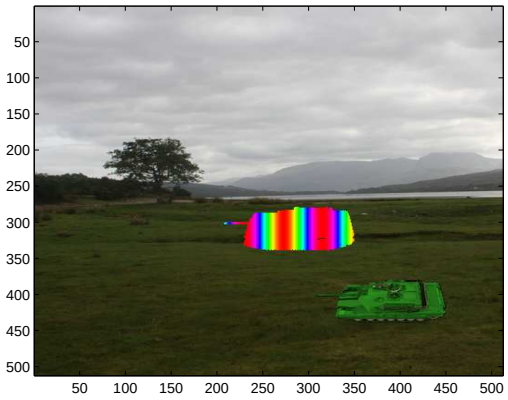

Fig. 11. An example input image showing the multicoloured target and a single colour target.

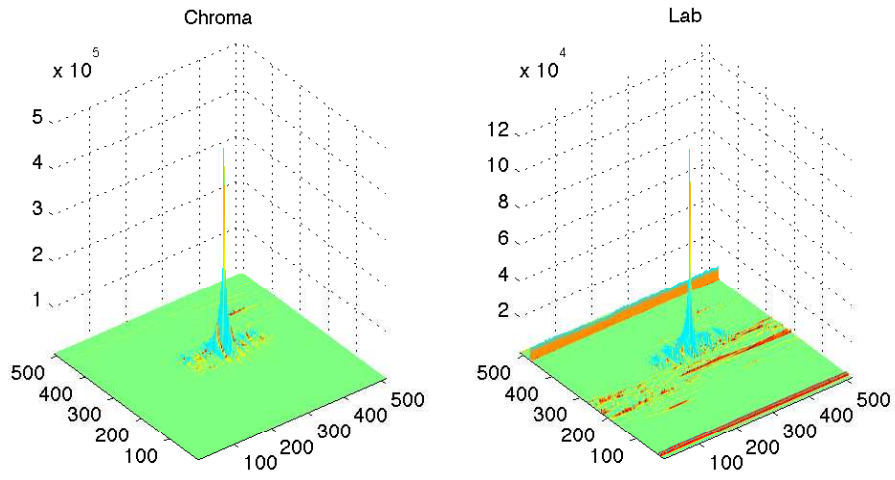

Fig. 12. An example results showing both the chroma and Lab encoding.

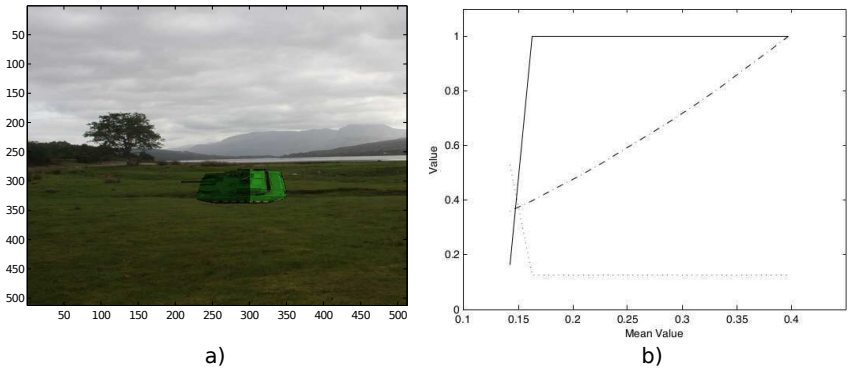

Fig. 13. a) A target tank with a shadow cast across it. b) Plot of the mean value versus COPA. The chroma encoded real COPA: solid line; chroma encoded imaginary COPA: Grey level correlation $\sqrt{\text{COPI}}$: dot dashed line

the correlator is shown in 12 for both colour spaces. Since the object has multiple colours equation 9 does not hold and the intensity of the output is sufficient to distinguish the objects.

4.A. Lighting invariance

The shadow rejection ability of the filter was tested by only altering the value across half of the tank image to produce a set of input images. Figure 13 a) show an example with the value multiplier set to 0.3 and giving a mean value across the tank of 0.21. This was repeated against a range of values as shown in figure 13 b) and compared against a grey level image correlation. The grey level correlation results are presented as the $\sqrt{\text{COPI}}$ so that they can be directly compared to the colour COPA.

4.B. Real World Result

The correlation technique has also been tested on real world images. Figure 14 a) shows a set of coloured plastic cogs and figure 14 b) shows the same image with a shadow cast across part of the image. A conventional DOg filtered grey level correlation was carried out using the middle left green cog as the target. The shadow was not present in the target image. The intensity in the correlation plane is shown in figure 15 a) without the shadow and in figure 15 b) with the shadow in the input.

The process was then repeated using the colour correlation technique. Figure 16 shows the correlation results split into real and imaginary components from chroma and Lab encoding with no shadow cast across the input. Figure 17 shows the same but with the shadow cast across the image. By examining the peaks in real component and ensuring its imaginary

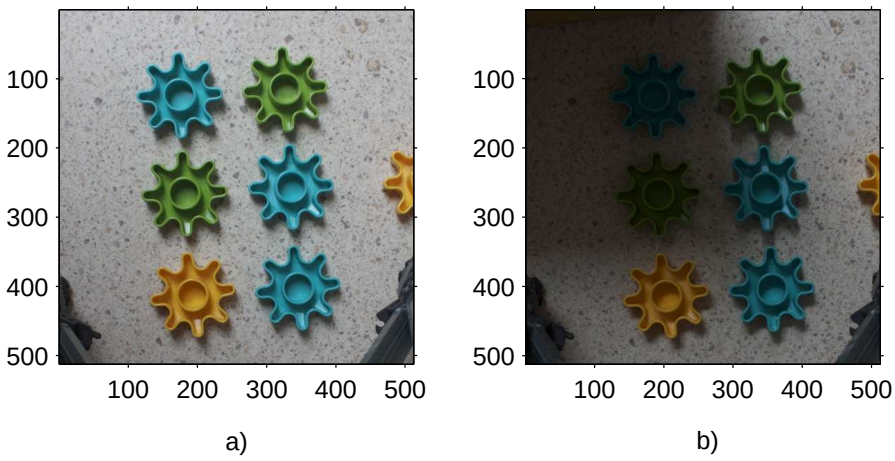

Fig. 14. a) Coloured plastic cogs. The green cogs are the target. b) Coloured plastic cogs with a shadow cast across some of them.

component is below $\alpha_{\mathbb{I}}$ the green coloured cogs can clearly be located in the shadowed and non-shadowed images.

4.C. Rotation invariance

The correlator implemented so far is not rotationally invariant and this is often desirable. There are a number of methods of achieving this such as: use circular harmonics [11]; use a series of composite filters such as the MACH filter and build the filter out of a set of rotated images [12–15] ; or use an alternative to the Cartesian space such as Log radius vs angle mapping [16]. The Log radius vs angle mapping has been implemented to demonstrate the rotation invariance. A single green tank was added to the background and this was re-mapped to the new space as described in [16]. The target tank was also remapped. The input tank was rotated in 5° steps and correlated using the chroma and Lab encoding. The peak height in the real and imaginary outputs are shown in figure 18. It can be seen that the encoding mechanisms can be implemented with a rotationally invariant filter.

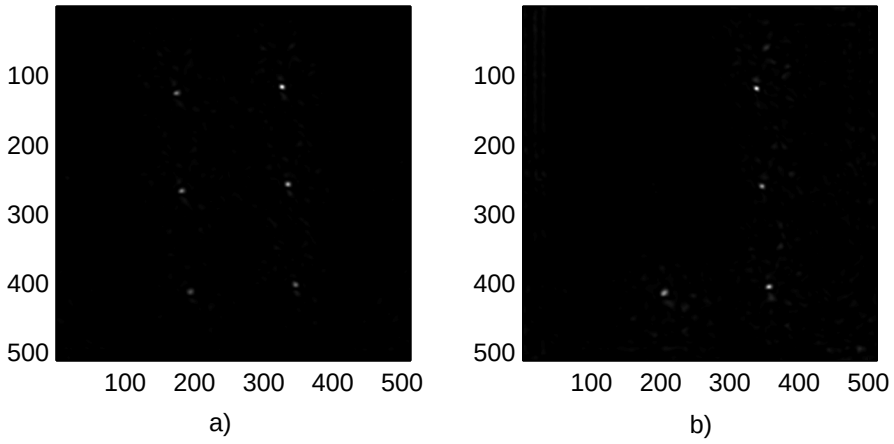

Fig. 15. a) Correlation output intensity for the grey scale correlator with figure 14 a) as the input. b)Correlation output intensity for the grey scale correlator with figure 14 b) as the input

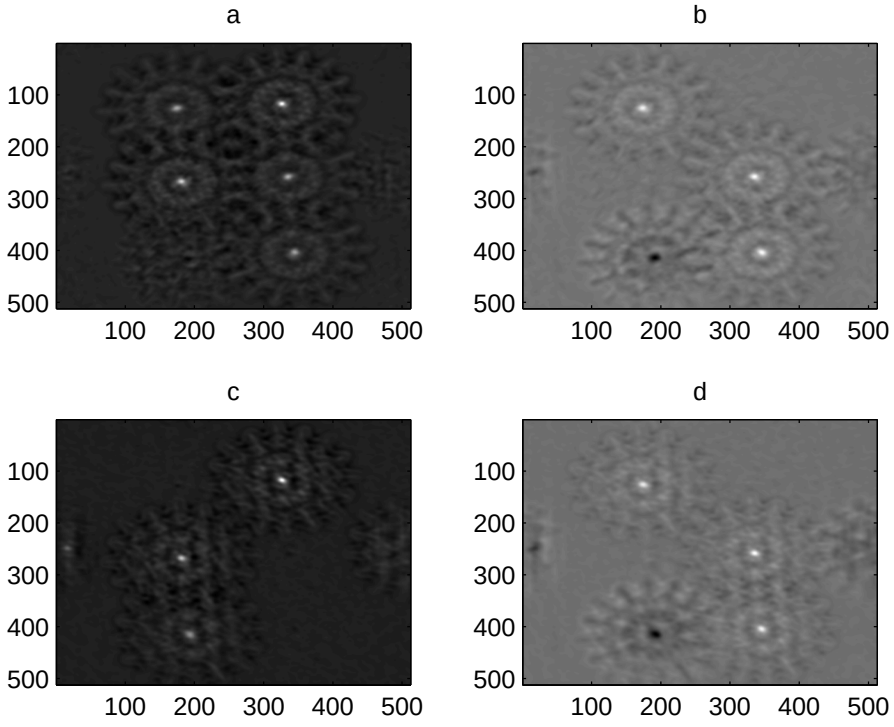

Fig. 16. Correlation output intensity with figure 14 a) as the input using the colour correlation method. a) Chroma real output, b) chroma imaginary output, c) Lab real output, d) Lab imaginary output. Black is zero in a) and c) and grey is zero in b) and d).

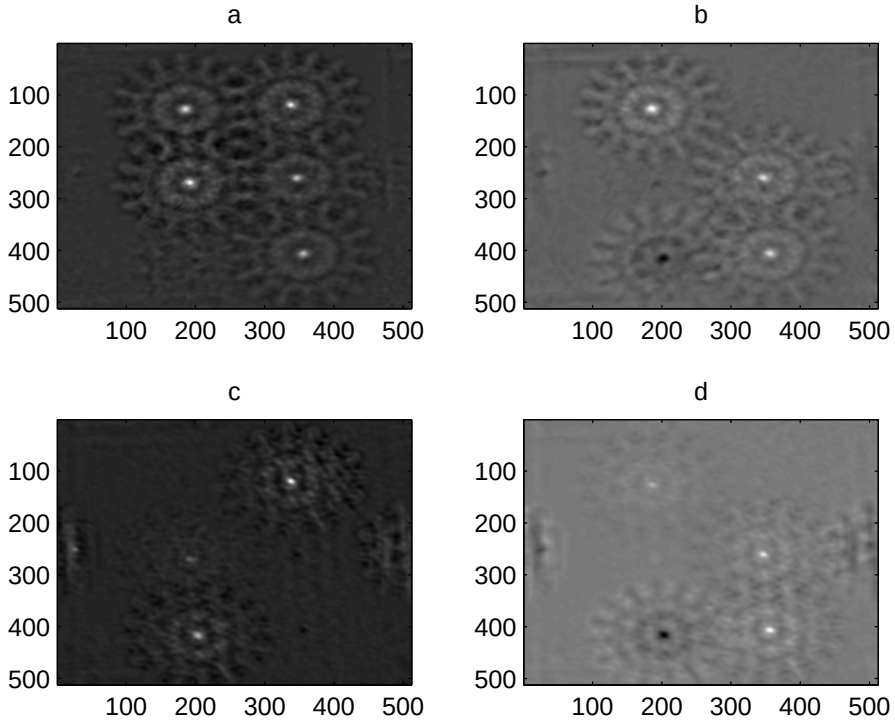

Fig. 17. Correlation output intensity with figure 14 b) as the input using the colour correlation method. a) Chroma real output, b) chroma imaginary output, c) Lab real output, d) Lab imaginary output. Black is zero in a) and c) and grey is zero in b) and d).

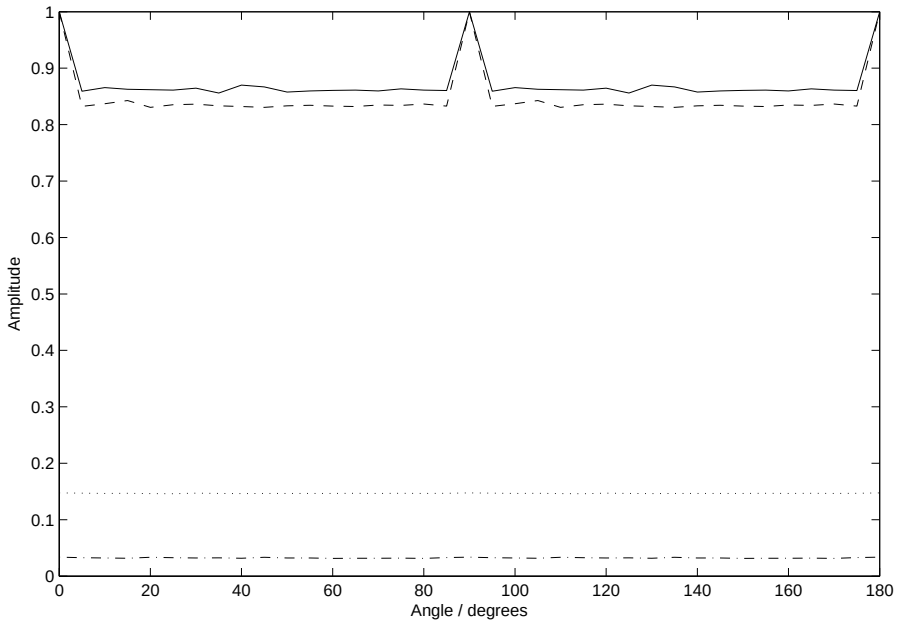

Fig. 18. The real and imaginary COPA versus the angle rotation of a green tank with a log radius versus angle mapping. The chroma encoded real COPA: solid line; chroma encoded imaginary COPA: dotted line; Lab encoded real COPA: dashed line; Lab encoded imaginary COPA: dot-dash line

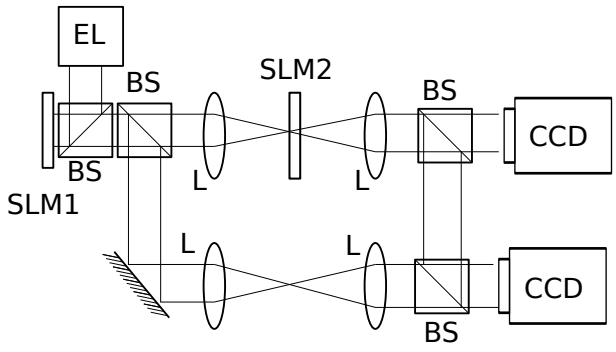

Fig. 19. Optical layout. EL - expanded laser, L - lens, BS - beam splitter, SLM1 reflective SLM, SLM2 - transmissive SLM, CCD - CCD cameras

5. Discussion

The results show how this encoding method can successfully be used to match not only the shape but the colour of an object. The method is perfectly realisable optically. This could be accomplished by using two SLMs or encoding on a carrier wave hologram such as in [17]. The measurement of the phase of the peak could be achieved interferometrically by either placing a 4-f correlator within the arm of a Mach-Zhender interferometer or by passing the output into a point diffraction interferometer [18]. An optical layout for such a experiment is shown in figure 19. The top CCD camera captures the correlation intensity image and the bottom CCD captures the There are many methods of implementing complex encoding using SLMs such as cascading two SLMs [19] or combining multiple pixels [20].

Out of the two colour encoding methods, the chroma exhibits the better rejection ability of different hues. This can be seen from the sharpness of the peaks in figure 10. Ideally we desire a large real component and small imaginary component for a match. Only the chroma encoding achieved this. Since the imaginary component must be less than $\alpha_{\mathbb{I}}$, the width of the colour class variation can be tuned. By setting $\alpha_{\mathbb{I}}$ to zero only a very narrow variation of hue will be accepted. Raising $\alpha_{\mathbb{I}}$ will allow more colour variation within the object.

Chroma encoding also has better brightness invariance than the Lab space. Figure 8 shows the chroma encoding has a fairly flat response to the changes in brightness. Neither encoding scheme cope well with changes in saturation as shown in figure 9. This is because as a colour datum de-saturates it moves towards the white regions of figures 1 a) and 1 b), and thus changes phase. Figure 9 shows a drop off in performance as the image loses colour information. A completely de-saturated image contains no colour and a conventional grey level correlator would be better in this situation

When multiple coloured object are used both the Lab and the chroma appear to work well

and experimentation suggests that the imaginary component can be ignored in this case. This will ease the implementation for an optical system since the interferometer arrangement shown in figure 19 can be replaced with a simpler 4-f correlator.

The relative failure of the Lab colour space to be fully brightness invariant can be attributed to the non-linear relationship with the CCD cameras response. Lab is calculated from converting the XYZ colour space into one that is uniform to human perception. Since this colour correlation is based on linear CCD responses, the Lab colour space does not perform as well as the chroma space.

Many grey level correlation techniques implement a band pass filter that tend to remove the low frequency terms. This is usually desirable since it edge enhances the image and removes global brightness variations. However, this also causes problems with shadows cast across the image. The edge of the shadow become a strong signal and compromises the correlation result. Figure 13 b) shows that by using chroma encoding the variation in brightness across the target object can be negated and thus this method significantly out performs the grey-level equivalent correlation.

The experiments using the images shown in figures 14 a) and 14 b) reinforces this. The conventional grey scale correlation can not distinguish between the coloured cogs as expected and shown in figure 15 a). It also fails when a large shadow is cast across the image as shown by the results in figure 15 b). This is because as a Fourier domain correlator the system can only remove the global brightness variations. However, when using the colour encoding technique the correlator performs much better at ignoring the local variation in brightness. In this example,since there is only a single colour in each cog, the rule for detection of the objects is the result must be positive and real only. It can be seen that the colour correlator locates the green cogs well using both Lab and chroma encoding.

In conclusion, a colour correlation technique has been presented that is extremely fast and simple to implement. Two colour spaces have been investigated and the chroma space appears to perform best. The technique is also invariant to the brightness of the illumination and shadows.

References

1. M. S. Millán, M. J. Yzuel, J. Campos, and C. Ferreira, "Different strategies in optical recognition of polychromatic images," Applied Optics **31**, 2560–2567 (5) (1992).
2. F. Yu, S. Jutamulia, R. Yelamarty, and D. Gregory, "Adaptive joint transform correlator for real-time colour pattern recognition," Optics & Laser Technology **21**, 185–188 (1989).
3. M. Hsieh, K. Hsu, and H. Zhai, "Color image recognition by use of a joint transform correlator of three liquid-crystal televisions," Applied Optics **41**, 1500–1504 (2002).

4. S. Sangwine, "Hypercomplex Fourier transforms of color images," IEEE International Conference on Image Processing, **1**, 137–140 vol.1 (2001).
5. B. Reddy and T. Prasad, "Color Image Registration and Template Matching Using Quaternion Phase Correlation," UbiCC Journal **6** (2011).
6. T. Ell and S. Sangwine "Hypercomplex Wiener-Khintchine theorem with application to color image correlation," , IEEE International Conference on Image Processing **2**, 792–795 vol.2 (2000).
7. W. Feng, B. Hu, and C. Yang, "A quaternion phase-only correlation algorithm for color images," , IEEE International Conference on Image Processing pp. 461–464 (2008).
8. C. Xie, M. Savvides, and B. Vijayakumar, "Quaternion Correlation Filters for Face Recognition in Wavelet Domain," IEEE International Conference on Acoustics, Speech, and Signal Processing, (ICASSP '05). **2**, 85–88 (2005).
9. L. JamalAldin, R. Young, and C. Chatwin, "Application of nonlinearity to wavelet-transformed images to improve correlation filter performance," Applied Optics **36**, 9212–9224 (1997).
10. P. Birch, B. Mitra, N. M. Bangalore, S. Rehman, R. Young, and C. Chatwin, "Approximate bandpass and frequency response models of the difference of gaussian filter," Optics Communications **283**, 4942 – 4948 (2010).
11. H. Arsenault and Y. Sheng, "Properties of the circular harmonic expansion for rotation invariant pattern recognition," Applied Optics **25**, 3225-3229 (1986).
12. B. V. K. Vijaya Kumar, L. Hassebrook, and L. Hostetler, "Linear phase coefficient composite filter banks for distortion-invariant optical pattern recognition," Optical Engineering **29**,1033-1043 (1990)
13. B. V. K. Vijaya Kumar, A. Mahalanobis, and A. Takessian, "Optimal tradeoff circular harmonic function correlation filter methods providing controlled in-plane rotation response," IEEE Trans. Image Process. **9**, 1025-1034 (2000)
14. V. R. Riasati and M. A. G. Abushagur, "Projection-slice synthetic discriminant functions for optical pattern recognition," Appl. Opt. **36**, 3022-3034 (1997).
15. S. Goyal, N. K. Nischal, V. K. Beri, and A. K. Gupta, "Wavelet modified maximum average correlation height filter for rotation invariance that uses chirp encoding in a hybrid digital optical correlator," Appl. Opt. **45**, 4850-4857 (2006).
16. P. Bone, R. Young, and C. Chatwin, "Position, rotation, scale and orientation invariant multiple object recognition from cluttered scenes," Optical Engineering **45**, 077203 (2006)
17. P. Birch, R. Young, C. Chatwin, M. Farsari, D. Budgett, and J. Richardson, "Fully complex optical modulation with an analogue ferroelectric liquid crystal spatial light modulator," Optics Communications **175**, 347 – 352 (2000).

18. R. N. Smartt and W. H. Steel, "Theory and application of point-diffraction interferometers," Japanese Journal of Applied Physics **14S1**, 351–356 (1975).
19. L. Neto, D. Roberge, and Y. Sheng, "Full-range, continuous, complex modulation by the use of two coupled-mode liquid-crystal televisions," Applied Optics **35**, 4567 – 4576 (1996)
20. S. Reichelt, R. Haussler, G. Fütterer, N. Leister, H. Kato, N. Usukura, and Y. Kanbayashi "Full-range, complex spatial light modulator for real-time holography," Optics Letters **37**, 1955 – 1957 (2012)